Electron mobility in tris(8-hydroxy-quinoline)aluminum thin films determined via transient electroluminescence from single- and multilayer organic light-emitting diodes

S. Barth, P. Müller, H. Riel, P. F. Seidler, and W. Rieß[a)]
IBM Research, Zurich Research Laboratory, Säumerstrasse 4, CH-8803 Rüschlikon, Switzerland

H. Vestweber
Covion Organic Semiconductors GmbH, Industrial Park Höchst, Building G 864, D-65926 Frankfurt am Main, Germany

H. Bässler
Institute of Physical-, Nuclear- and Macromolecular Chemistry and Center of Material Science, Philipps-University of Marburg, Hans-Meerwein-Strasse, D-35032 Marburg, Germany

(Received 8 June 2000; accepted for publication 9 October 2000)

Transient electroluminescence (EL) from single- and multilayer organic light-emitting diodes (OLEDs) was investigated by driving the devices with short, rectangular voltage pulses. The single-layer devices consist of indium-tin oxide (ITO)/tris(8-hydroxy-quinoline)aluminum (Alq_3)/magnesium (Mg):silver (Ag), whereas the structure of the multilayer OLEDs are ITO/copper phthalocyanine (CuPc)/N,N′-di(naphthalene-1-yl)-N,N′-diphenyl-benzidine (NPB)/Alq_3/Mg:Ag. Apparent model-dependent values of the electron mobility (μ_e) in Alq_3 have been calculated from the onset of EL for both device structures upon invoking different internal electric field distributions. For the single-layer OLEDs, transient experiments with different dc bias voltages indicated that the EL delay time is determined by the accumulation of charge carriers inside the device rather than by transport of the latter. This interpretation is supported by the observation of delayed EL after the voltage pulse is turned off. In the multilayer OLED the EL onset—dependent on the electric field—is governed by accumulated charges (holes) at the internal organic-organic interface (NPB/Alq_3) or is transport limited. Time-of-flight measurements on 150-nm-thin Alq_3 layers yield weak field-dependent μ_e values of the order of $1\times10^{-5}\,cm^2/Vs$ at electrical fields between 3.9×10^5 and 1.3×10^6 V/cm. © *2001 American Institute of Physics.*
[DOI: 10.1063/1.1330766]

I. INTRODUCTION

Since the first observation of efficient bright emission from a triphenylamine derivative/tris(8-hydroxy-quinoline) aluminum (Alq_3) bilayer structure,[1] organic light-emitting diodes (OLEDs) have been studied extensively due to their potential application in flat-panel displays.[2–9] Besides efficiency, long-term stability, peak brightness and stability under high driving conditions, the response time of OLEDs is an essential criterion for their application in such thin-film displays. The response time, i.e., the time lag between addressing the device by a short, rectangular voltage pulse and the first appearance of electroluminescence (EL), is determined by the superposition of various elementary electronic processes: charge-carrier injection, charge-carrier transport, buildup of space charges, formation of the excited state, and the radiative decay of the excited state. It is usually difficult to disentangle these electronic processes. One way to do so involves time-resolved studies, e.g., transient EL measurements. Time-resolved EL experiments have already been successfully applied to organic crystals,[10,11] low-molar-mass organic compounds,[12–23] and polymeric materials.[24–45] However, the interpretation of the results often turns out to be difficult. In a single-layer OLED the time-dependent EL onset, also called the delay time t_d, is identified as the time until the two leading fronts of injected carriers—holes and electrons—meet in the device. The time after the EL tends to saturate (rise time t_r) is the time until electron and hole distributions have interpenetrated, which is controlled by the charge-carrier motion into the bulk of the sample. In a bi- or multilayer structure the situation is even more complicated because of possible charge-carrier accumulation at the internal interface or interfaces, respectively. In bilayer structures, for example, t_d is the time until the leading front of the charge carriers with the lowest mobility (minority carriers)—in most cases electrons—reach the internal organic–organic interface and recombine with the first injected opposite charge carriers—in most cases holes—waiting at the interface, whereas t_r reflects the buildup of the minority carrier density in the recombination zone. The temporal decay pattern of the EL at the end of the applied voltage pulse reflects the depletion of the charge-carrier reservoir established during the preceding on-phase. The corresponding EL signal differs in a characteristic way for single and bi- or multilayer devices. Whereas in the former the EL decays

a)Electronic mail: wri@zurich.ibm.com

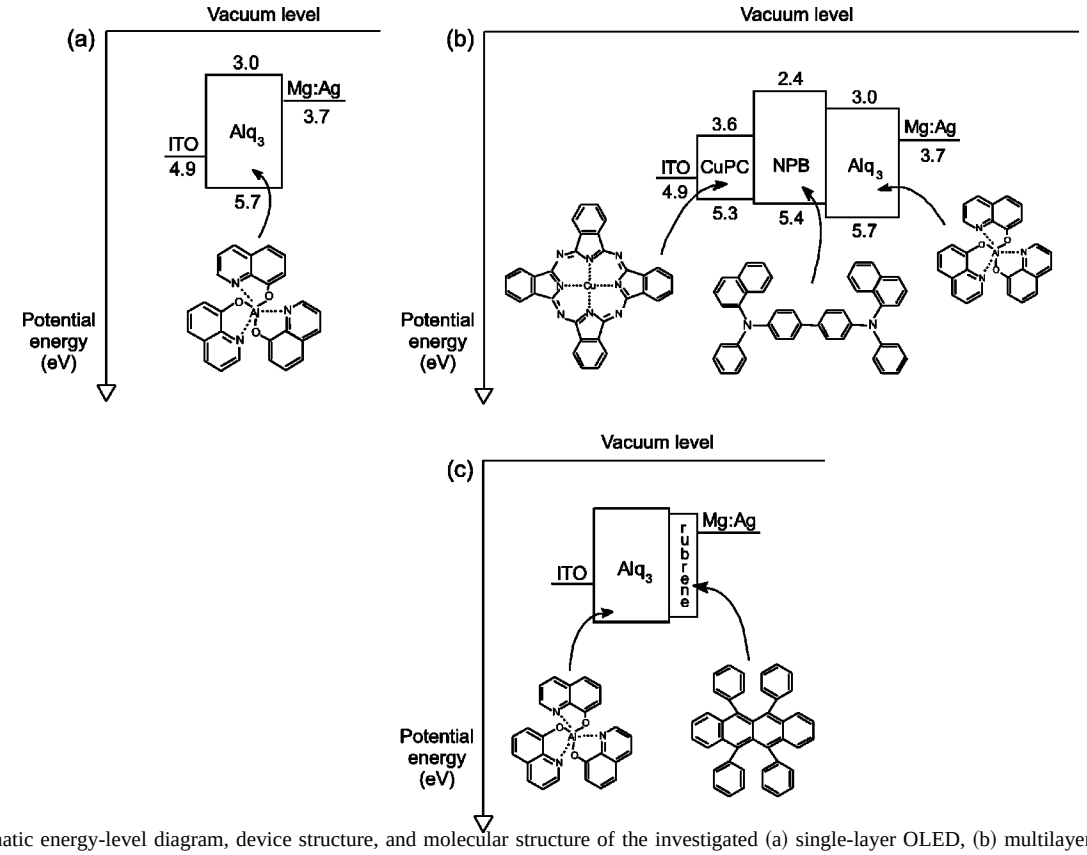

FIG. 1. Schematic energy-level diagram, device structure, and molecular structure of the investigated (a) single-layer OLED, (b) multilayer OLED, and (c) sample used for TOF measurements.

monotonously, the latter structures often feature an EL overshoot following the end of the voltage pulse.[46]

It is common practice that in single-layer devices the onset of EL is interpreted as being the transit time (t_{tr}) of the majority charge carriers. However, it has been found that the mobility values obtained via t_d, from single as well as bilayer systems, are orders of magnitude lower than those determined from time-of-flight (TOF) measurements, especially at low voltages.[15,28,30] This discrepancy was attributed to the accumulation of space charges at interfacial barriers, which have a major effect on t_d in time-resolved EL experiments. This interpretation was recently confirmed for a bilayer device by an analytical theory.[47] It has been shown that the EL onset is governed by the growth of the interfacial charge densities and the concomitant redistribution of the electric field inside the sample rather than by charge-carrier transport. Therefore, it is all but straightforward to identify t_d with t_{tr}. However, transient EL measurements have the advantage that they provide information directly from the emitting device. So far there exists no detailed TOF investigations under operation conditions of OLEDs, i.e., in devices with a typical thickness of 100 nm and under the action of electric fields exceeding 10^6 V/cm, to determine the charge-carrier mobilities in such thin films.

In this work we report on transient EL measurements of multilayer OLEDs, which consist of indium-tin oxide (ITO)/copper phthalocyanine (CuPc)/N,N′-di(naphthalene-1-yl)-N,N′-diphenyl-benzidine (NPB)/Alq_3/magnesium (Mg):silver (Ag). In order to investigate the mechanism of the time evolution of the EL in single-layer devices, we performed experiments on an ITO/Alq_3/Mg:Ag OLED. Transient experiments with different dc bias voltages and investigations of the EL decay behavior were performed to clarify the influence of space charges on the EL onset. In addition we present TOF measurements on a 150-nm-thin Alq_3 film to determine the electron mobility in Alq_3 under operation conditions of OLEDs and to compare these results with mobility values calculated from time-resolved EL experiments.

II. EXPERIMENT

Our single-layer OLEDs consist of glass substrates (7059 Corning) covered with a patterned ITO anode (surface resistance 45 Ω/square, 80-nm thickness), followed by a 100-nm-thin Alq_3 layer as active material and finally a Mg:Ag (10:1) alloy as metal top cathode. The structure of the multilayer OLEDs is ITO as anode, CuPc as buffer layer, NPB as hole transport layer, Alq_3 as electron transport and emitting layer, and a Mg:Ag (10:1) alloy as cathode. The devices for the TOF measurements consist of ITO, Alq_3 as charge-transport layer (CTL), 5, 6, 11, 12-tetraphenylnaphthacene (rubrene) as charge-generation layer (CGL), and Mg:Ag (10:1) as counterelectrode. The schematic device structures together with the energy-level diagrams and the molecular structures of the materials used are shown in Figs. 1(a)–1(c).

All layers were prepared in a high-vacuum system (Leybold) by vapor deposition using resistively heated tantalum and tungsten boats. The base pressure in the chamber ranged between 4×10^{-7} and 2×10^{-6} mbar. The typical deposition

rate for the organic materials and the metals was about 1 Å/s. For the deposition of the Mg:Ag alloy the evaporation rates of Mg and Ag were controlled independently by separate thin-film deposition monitors (Leybold Infikon). The active area of our devices was 2×2 mm^2. The evaporation chamber was attached directly to a glovebox, which allows device fabrication, first characterizations, encapsulation, and storage of the devices completely under inert (argon) conditions.

For the transient EL experiments we used a HP 8116A DC pulse/function generator (50 MHz, rise time $\cong$7 ns, decay time $\cong$10 ns) to apply rectangular voltage pulses to our devices. The repetition rate of the pulses was 1 kHz, and the pulse length varied between 5 and 10 μs. In addition the function generator permitted us to drive the OLEDs with various offset voltages before applying the rectangular voltage pulses. The encapsulated devices were fixed in a customized HP 16058A test fixture together with a Hamamatsu photomultiplier 5783-01 (time resolution $\cong$0.65 ns) located directly on top of the emitting area to detect the EL intensity. The photomultiplier was connected to the 50-Ω input resistance of a digital oscilloscope (Tektronix 2440, sampling rate: 500 MS/s, resolution: 200 μV) to record the time-dependent EL signals. Our experimental setup allowed us to detect with a second digital oscilloscope (Tektronix 2440) the applied voltage pulse and the time-dependent cell current through the devices simultaneously with the EL signal. Both oscilloscopes were connected to a personal computer for the transfer and evaluation of the experimental data. The RC time constant of the setup, including the OLED device, was $\cong$0.2 μs.

The transient photocurrents were recorded with the TOF technique.[48] The charge carriers were generated in a 10-nm-thin rubrene layer, which served as CGL, by illumination through the ITO anode with pulses of a Nd:YAG pumped optical parametric oscillator (OPO) (Spectra Physics GCR 170 and MOPO 710) driven at 530 nm (pulse duration=8 ns, repetition rate=10 Hz). The photocurrents were amplified by a low noise current amplifier (HVA, FEMTO Messtechnik) and recorded by a digital oscilloscope (Tektronix TDS 640 A, 500 MHz, sampling rate: 2 GS/s). To avoid space-charge accumulation in the device the excitation density was chosen to limit the emitted charge to 0.05 CU, where C is the device capacitance and U is the applied voltage. After each measurement the sample was shorted and kept in the dark for a few minutes before the next signal was taken. During the measurements the device was held in a cryostat under vacuum ($\cong10^{-5}$ mbar). All experiments—transient EL and TOF—were performed at room temperature (295 K).

III. RESULTS

Figure 2 presents the transient behavior of the EL of an ITO/CuPc (20 nm)/NPB (45 nm)/Alq_3 (50 nm)/Mg:Ag multilayer OLED upon applying a rectangular voltage pulse of 16 V. The pulse length was 5 μs, the repetition rate 1 kHz, and the EL signal was averaged over 256 samples. The EL onset occurred with a delay time of $\cong$0.48 μs. For $t>t_d$ the EL signal increased and tended to saturate after $\cong$1.76 μs, defined by the intercept of the tangents. For comparison the cell current is also plotted in Fig. 2. The voltage dependence of the transient EL of the multilayer structure is shown Fig. 3. With increasing voltage a decreasing delay time and a steeper rise of the EL was observed. At the beginning and end of the applied voltage pulses, weak parasitic effects—negative and positive peaks—occurred in the EL signal (Figs. 2 and 3), which are caused by capacitive coupling effects. In Fig. 4(a) a typical function generator output signal of 10-μs pulse width is presented. The corresponding EL signal together with the cell current of an ITO/Alq_3 (100 nm)/Mg:Ag single-layer OLED is shown in Fig. 4(b) detected under the same experimental conditions as for the multilayer device in Fig. 2. The EL grows after $\cong$0.64 μs and t_r is determined to be $\cong$2.32 μs. Figure 5 presents the time-resolved EL of the single-layer structure parametric in the applied voltage. With increasing voltage a decreasing EL onset and a steeper rise of the EL is observed, equivalent to a faster response time of the OLED. Note that t_d and t_r exceed the values measured with the multilayer device. The transient EL behavior of the single-layer OLED upon applying different positive and negative offset voltages before the rectangular voltage pulse is shown in Fig. 6 (positive voltage refers to the ITO electrode). The pulse length was 10 μs and

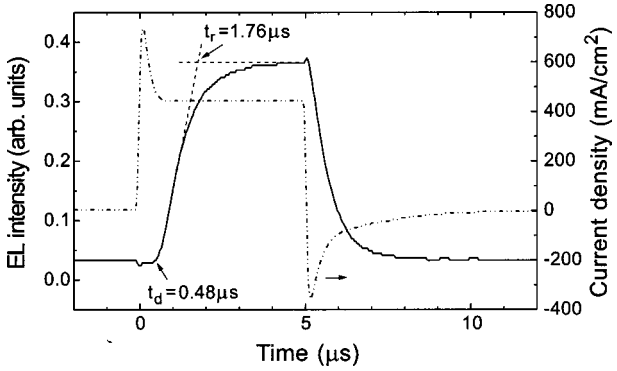

FIG. 2. Comparison between time response of EL and cell current in an ITO/CuPc (20 nm)/NPB (45 nm)/Alq_3 (50 nm)/Mg:Ag multilayer OLED upon application of a rectangular voltage pulse of 16 V with a pulse length of 5 μs and a repetition rate of 1 kHz. The EL signal was averaged over 256 samples.

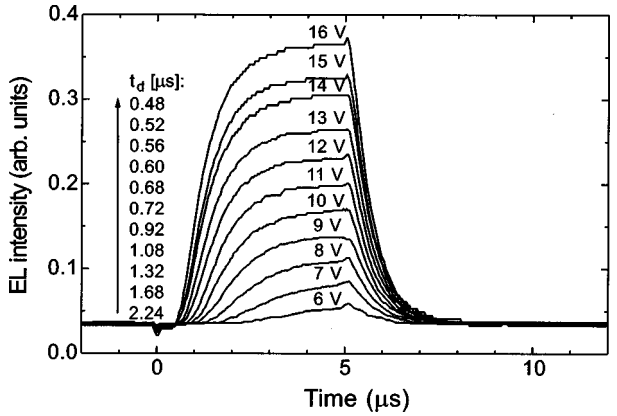

FIG. 3. Voltage dependence of the transient EL from an ITO/CuPc (20 nm)/NPB (45 nm)/Alq_3 (50 nm)/Mg:Ag multilayer OLED. The pulse width was 5 μs and the repetition rate 1 kHz.

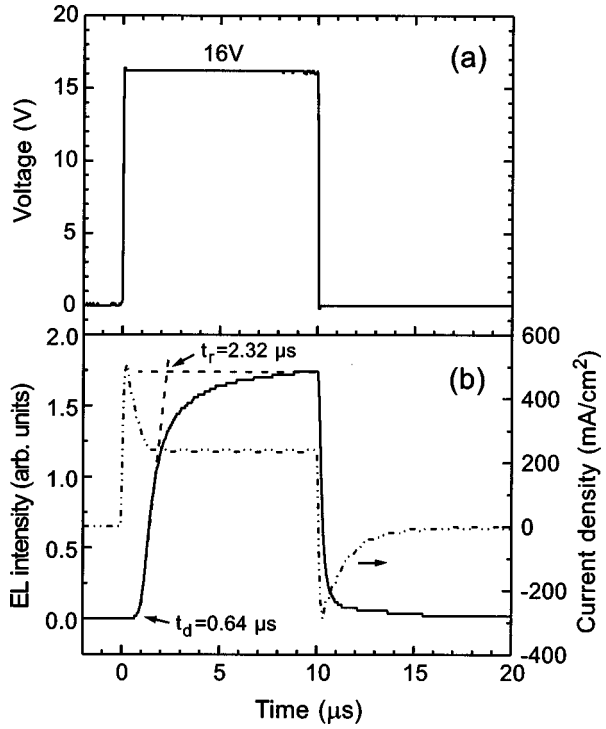

FIG. 4. (a) Typical function generator output signal of 10-μs pulse length. (b) Comparison between transient EL and cell current in an ITO/Alq_3 (100 nm)/Mg:Ag single-layer OLED upon application of a rectangular voltage pulse of 16 V. The pulse length was 10 μs, the repetition rate 1 kHz, and the EL was averaged over 256 samples.

the repetition rate 1 kHz. Both t_d and t_r are influenced by different dc bias voltages. With increasing negative offset voltages t_d and t_r increase, whereas increasing positive offset voltages lead to decreasing t_d and t_r. The inset depicts an enlargement of the EL decay behavior for the various offset voltages. Figure 7 presents a detailed investigation of the EL decay of an ITO/Alq_3 (100 nm)/Mg:Ag sample after the voltage pulse has been turned off. The EL decay signal is nonexponential and can be represented by two exponential decays with time constants of $\cong$0.3 μs and $\cong$10 μs, respectively. Figure 8 shows a typical TOF signal of an ITO/Alq_3 (150 nm)/rubrene (10 nm)/Mg:Ag device obtained

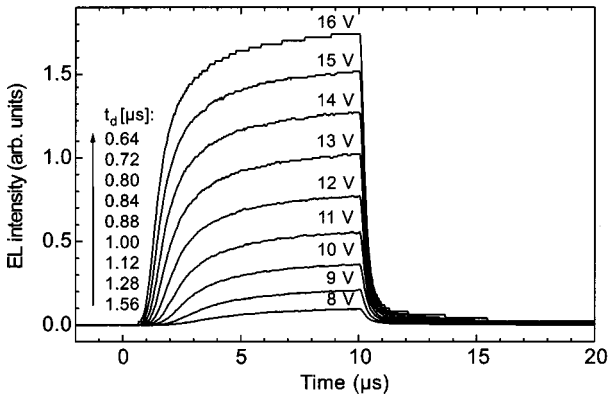

FIG. 5. Voltage dependence of the time-resolved EL from an ITO/Alq_3 (100 nm)/Mg:Ag single-layer device. The pulse length was 10 μs and the repetition rate 1 kHz.

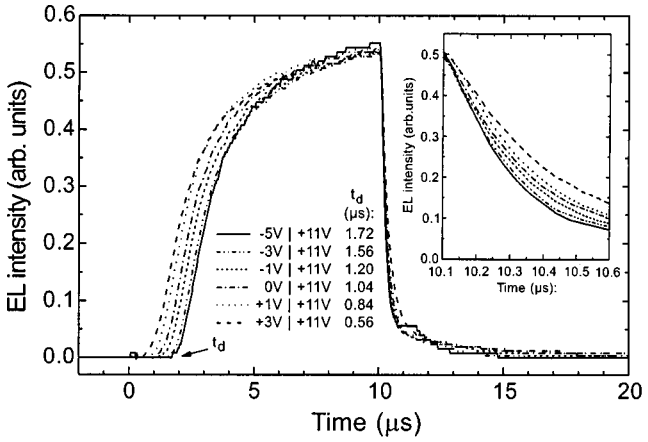

FIG. 6. Comparison of the time response of EL from an ITO/Alq_3 (100 nm)/Mg:Ag OLED upon application of various offset voltages, between -5 and $+3$ V, before a 10-μs-long rectangular pulse was applied with a repetition rate of 1 kHz. Inset: expanded view of the EL decay signals for the various applied offset voltages.

at an electric field of 5.9×10^5 V/cm. In Fig. 8(a) the dispersive current transient is plotted in a double linear representation and in Fig. 8(b) on a double logarithmic scale. In the latter figure t_{tr} is determined from the intersection of the asymptotes to the current transient to be $\cong$1.1 μs. In addition the time required for the current to decrease to one-half of its value at t_{tr} is shown ($t_{1/2}\cong2.4\,\mu$s).

IV. DISCUSSION

First we shall discuss the time-resolved behavior of the EL of an ITO/CuPc (20 nm)/NPB (45 nm)/Alq_3 (50 nm)/Mg:Ag multilayer OLED. The energy-level diagram under flat band conditions[49,50] portrayed in Fig. 1(b) clearly proves the existence of energy barriers for both electrons and holes at the NPB/Alq_3 interface. Therefore the observed green emission[51] from the device (peak maximum at about 515 nm, color coordinates 0.30, 0.52) can be attributed to the recombination of accumulated holes and electrons at this interfacial layer. It is also straightforward to associate the transient EL

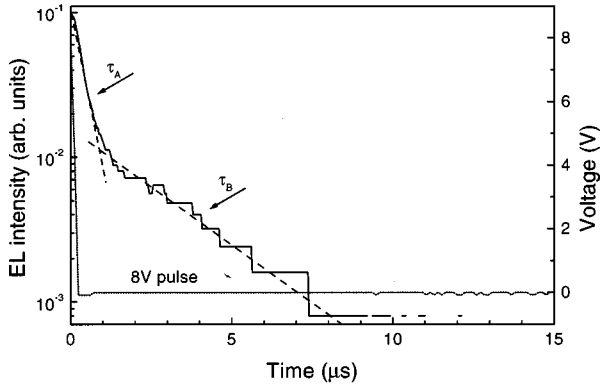

FIG. 7. EL decay behavior at the trailing edge of a 10-μs-long rectangular 8-V pulse from an ITO/Alq_3 (100 nm)/Mg:Ag single-layer structure on a semilogarithmic scale. The EL decay is nonexponential and can be described as the sum of two exponential decays with time constants of $\tau_A\cong0.3\,\mu$s and $\tau_B\cong10\,\mu$s, respectively.

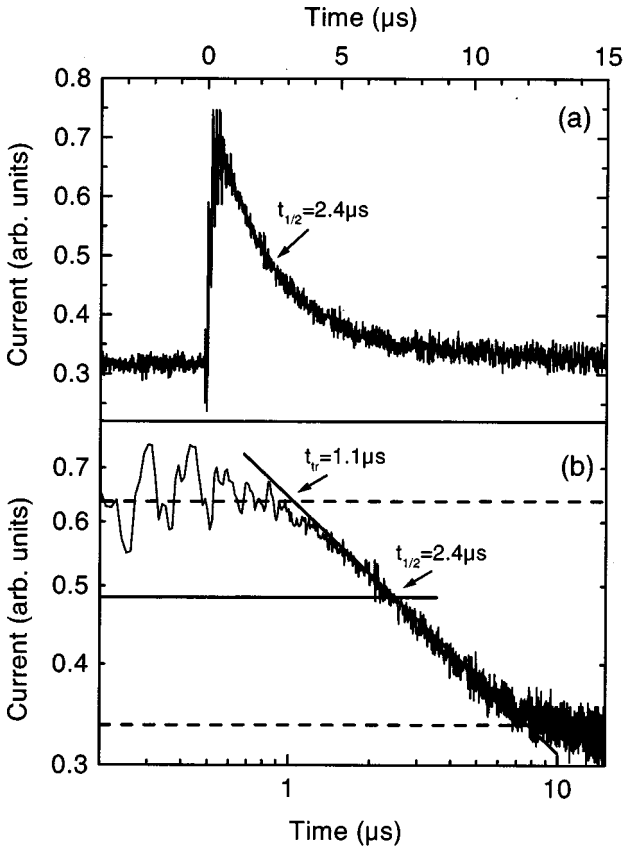

FIG. 8. Typical current transient from an ITO/Alq_3 (150 nm)/rubrene (10 nm)/Mg:Ag device in (a) a double linear and (b) double logarithmic representation at $E=5.9\times10^5$ V/cm. The excitation was through the positively biased ITO electrode at $\lambda_{exc}=530$ nm. Via the intersection of the asymptotes to the plateau and to the trailing edge of the current transient, t_{tr} is determined to be 1.1 μs. Additionally marked is the time required for the current to decrease to one-half of its value at $t_{tr}(t_{1/2}=2.4\,\mu s)$; $\mu_e=2.3\times10^{-5}$ cm^2/Vs (via t_{tr}) and $\mu_e=1.1\times10^{-5}$ cm^2/Vs (via $t_{1/2}$).

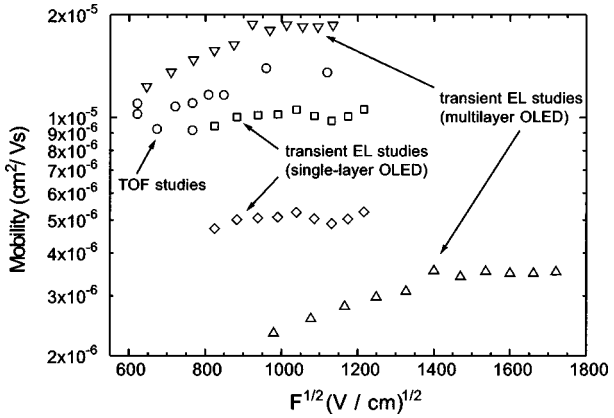

FIG. 9. Electric-field dependence for upper and lower bounds of the apparent electron mobility in Alq_3 calculated via t_d from time-resolved EL measurements: for the ITO/CuPc (20 nm)/NPB (45 nm)/Alq_3 (50 nm)/Mg:Ag multilayer OLED, assuming that one of the following limiting cases occurs, (a) there exists a homogeneous electrical field within the complete device structure (down triangles) or (b) the entire electric field drops across the Alq_3 layer (up triangles); for the ITO/Alq_3 (100 nm)/Mg:Ag single-layer OLED under the assumptions (a) $\mu_e \gg \mu_h$ (squares) and (b) $\mu_e=\mu_h$ (diamonds). For comparison μ_e values from TOF measurements of an ITO/Alq_3 (150 nm)/rubrene (10 nm)/Mg:Ag device calculated via $t_{1/2}$ are presented (circles). $U_{bi}=1.2$ V was considered for all calculations, i.e., transient EL and TOF.

behavior with this interfacial charging. However, one has to clarify whether the buildup of space charges at the NPB/Alq_3 interface determined the EL onset in the entire electric field range investigated or merely modified t_d in a part of this range where, for example, the charge-carrier transport can predominate.

In Fig. 9 it is shown that for applied rectangular voltage pulses $\leqslant$10 V [i.e., $F^{1/2}\leqslant880$ (V/cm)$^{1/2}$ (case a) and $F^{1/2}\leqslant1340$ (V/cm)$^{1/2}$ (case b)] the calculated electron mobilities (μ_e) are field dependent, whereas for $\geqslant$11 V [i.e., $F^{1/2}\geqslant920$ (V/cm)$^{1/2}$ (case a) and $F^{1/2}\geqslant1400$ (V/cm)$^{1/2}$ (case b)] μ_e is field independent. The latter indicates that at higher electrical fields t_d is limited by charge-carrier transport and at lower fields by space charges due to accumulated holes and electrons at the NPB/Alq_3 interface. A detailed analysis of t_d (for low electric fields) as a function of the cell current j yields an inverse relationship between t_d and j, i.e., t_d decreases with increasing j. In addition the product jt_d is of the same order of magnitude as $C_{Alq_3}\cdot U$ (a few 10^{-9} As). Both results indicate that t_d reflects the time needed to accumulate a space-charge layer at the internal interface rather than the transit time of charge carriers. Taking into account that holes are the majority carriers in our multilayer OLED and j is proportional to $1/t_d$, we conclude that holes are responsible for the accumulation of charge carriers at the NPB/Alq_3 interface. A further argument against attributing t_d for applied voltage pulses $\leqslant$10 V to a carrier-transit time is the relatively large variation of t_d upon varying the height of the applied voltage pulse and the lack of a saturation behavior of t_d within this electric field regime (Fig. 3). Comparable results have been reported previously for a polymeric bilayer LED.[31] More comprehensive studies of EL transients from the above-mentioned multilayer OLED at lower electrical fields can be found in Ref. 52.

The same relationship between t_d and j is obtained for the high electrical-field range, but t_d tends to saturate with increasing j, and jt_d is no longer of the same order of magnitude as $C_{Alq_3}\cdot U$. Again this proves that accumulated charges (holes) at the NPB/Alq_3 interface play a minor role at higher fields—although they are present—and that t_d is governed by charge-carrier transport. Such a saturation of t_d is also observed with different dc bias voltages, where t_d shows a tendency to reach a constant value as the offset voltage increases.

It should be mentioned that the peaks in the cell-current signal at the beginning and end of the applied voltage pulse (Fig. 2) are caused by the charging and discharging of the OLED, which can be treated as a capacitor, and the rise time t_r determined by the intercept of the tangents (Fig. 2) reflects saturation of the electron-carrier density in the recombination zone, i.e., at the NPB/Alq_3 interfacial layer.

Next we calculate the electron mobility in Alq_3 via t_d from the multilayer OLED (Fig. 3). Usually the charge-carrier mobility μ is given by $\mu=L/(t_{tr}F)$ with $F=(U-U_{bi})/d$, where F is the electric field, L is the thickness of the active material, U is the voltage applied to the device, and U_{bi} is the built-in voltage calculated from the difference

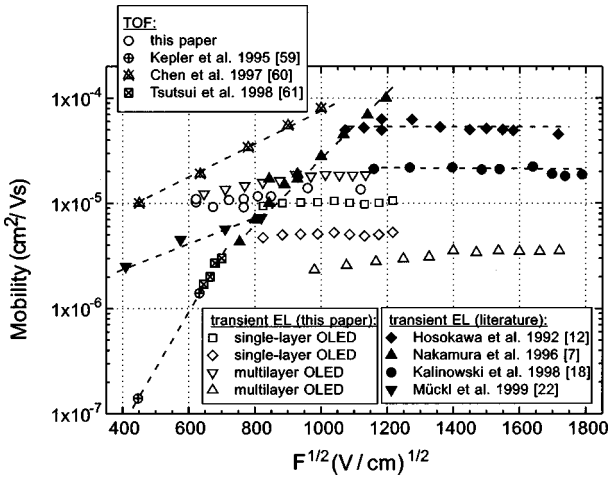

FIG. 10. Comparison of the electric-field dependence of μ_e in Alq_3 calculated in this article from time-resolved EL and from TOF results (see Fig. 9) with data published in the literature. The latter were obtained via transient EL measurements from the following device structures: ITO/TPD (60 nm)/Alq_3 (60 nm)/Mg:Ag (Hosokawa *et al.*[12] and Kalinowski *et al.*[18]), ITO/TPD (60 nm)/Alq_3 (60 nm)/Ca (Mückl *et al.*[22]), and ITO/MTDATA (60 nm)/TPD (20 nm)/Alq_3 (60 nm)/Mg:Ag (Nakamura *et al.*[7]). The TOF studies were performed with the following device structures: Si/Alq_3 (400 nm)/Al (Kepler *et al.*[55]) and Si/Alq_3 (200 nm)/Au (Chen *et al.*[60]).

of the work functions of ITO and Mg:Ag alloy ($U_{bi} \cong 1.2$ V). Before going into more detail we have to point out that by using t_d instead of t_{tr} (transit time obtained via TOF measurements) in the above-mentioned equation we can only obtain *apparent* values for the charge-carrier mobilities because t_d is determined by the buildup of space charges inside the devices, and/or the charge-carrier transport behavior, dependent on the electric-field range investigated. The accumulation of holes at the NPB/Alq_3 interface in the multilayer device, as discussed above, leads to a redistribution of the electric field inside the device in such a manner that the field in the electron-transport layer (Alq_3) increases and the field in the hole-transport layer (NPB) decreases. Therefore the actual electrical-field distribution in the multilayer OLED is unknown. From t_d one can only determine upper and lower bounds of the *apparent*, only operationally defined electron mobility μ_e in Alq_3 for the limiting cases that (a) there exists a homogeneous electrical field within the complete device structure or (b) the entire electrical field drops across the Alq_3 layer. Under these assumptions, μ_e in Alq_3 is between $1.2-1.9\times10^{-5}$ cm^2/Vs (case a) and $2.3-3.5\times10^{-6}$ cm^2/Vs (case b) for electric fields ranging between 4.2×10^5 and 3.0×10^6 V/cm (Fig. 9). In Fig. 10 we compare these calculated *apparent* μ_e values with those published in the literature. Hosokawa *et al.*[12] and Kalinowski *et al.*[18] presented data from an ITO/N,N′-diphenyl-N,N′-bis(3-methylphenyl)-(1,1′-biphenyl)-4,4′-diamine (TPD) (60 nm)/Alq_3 (60 nm)/Mg:Ag bilayer OLED. They performed transient EL measurements and calculated indirect values for μ_e in Alq_3 via t_d under the simplified assumption that there exists a homogeneous electric-field distribution (corresponding to our case a) inside their devices, despite the presence of the TPD/Alq_3 interfacial layer. As shown in Fig. 10 the calculated electron mobilities of both groups are field independent in the high field range. Whereas the data of Kalinowski *et al.*[18] can be treated as a continuation of our results to higher electric fields, those of Hosokawa *et al.*[12] differ only by a factor of 2 to 3. However, in both studies U_{bi} was not considered. Mückl *et al.*[22] investigated the low field range of the above-mentioned bilayer structure with the same active layer thicknesses, but with a calcium cathode. For the calculation of μ_e they took into account the built-in field (U_{bi}) of their device and assumed a drop of the entire electrical field across the Alq_3 layer (corresponding to our case b). They ended up with a field dependence of μ_e in the low field regime that correlates with our results. However, the data presented by Nakamura *et al.*[7] from an ITO/4,4′,4″-tris(N-(*m*-tryl)-N-phenyl-amino)-triphenylamine (MTDATA) (60 nm)/TPD (20 nm)/Alq_3 (60 nm)/Mg:Ag OLED strongly differ from our and all other published μ_e values. These authors assumed a uniformly applied electric field over the entire device (our case a) and observed a pronounced field dependence of μ_e both in the low and high electric-field regime. The built-in voltage, however, was not taken into consideration in their calculations.

To investigate the mechanism that determines the time evolution of EL in single-layer OLEDs we performed transient EL measurements with an ITO/Alq_3 (100 nm)/Mg:Ag structure as shown in Figs. 4(b) and 5. At first sight it is striking that t_d and t_r exceed the values measured for the multilayer device. The shorter response time of the latter can be attributed to an improved injection efficiency due to the lowering of the injection barrier by inserting a thin CuPc layer between ITO and NPB.[50] A detailed study of the influence of such an interface grading in the multilayer device used in this work can be found in Ref. 53. In addition one has to keep in mind that in the multilayer OLED the accumulation of holes [μ_h(NPB)$\cong10^{-3}$ cm^2/Vs,[54] i.e., μ_h(NPB)$\gg\mu_e$(Alq_3)] at the NPB/Alq_3 interface enhances the electric field inside the Alq_3 layer and therefore results in an improvement of the electron-injection efficiency. The recombination zone of electrons and holes in our single-layer OLED lies near the ITO anode because of the higher injection barrier for holes and their approximately two orders of magnitude lower mobility in Alq_3.[22,55] Therefore a further argument for the longer response time of the latter is the more than 60% greater Alq_3 layer thickness, which electrons have to cross before recombining radiatively with the first injected holes.

In principle, in single-layer OLEDs t_d reflects the time when the two leading fronts of injected carriers—electrons and holes—meet in the sample, whereas t_r can be attributed to the time until electron and hole distributions have interpenetrated. The latter is controlled by the charge-carrier motion into the bulk of the device. An open question is which process prevails, i.e., the control of t_d by charge-carrier transport or by the accumulation of charges. Therefore the calculated values of the *apparent* electron mobility in the Alq_3 range from 9.4×10^{-6} to 1.1×10^{-5} cm^2/Vs, assuming $\mu_e\gg\mu_h$, and $4.7-5.3\times10^{-6}$ cm^2/Vs assuming $\mu_e=\mu_h$ at electric fields varying between 6.8×10^5 and 1.5×10^6 V/cm (Fig. 9). An answer to this question is provided by transient

EL measurements in the single-layer device upon applying different positive or negative offset voltages before admitting the rectangular voltage pulse (Fig. 6). With increasing negative offset voltage t_d increases and with increasing positive offset voltage t_d decreases. These results indicate that even without an apparent internal organic–organic interface t_d is determined by the accumulation of space charges and the concomitant redistribution of the electric field inside the device rather than by charge-carrier transport. Otherwise t_d should not vary with dc bias voltages. A more precise look at the EL decay behavior (inset of Fig. 6) indicates a slow decrease of the EL decay with increasing the offset voltage, which clearly proves a charging of our device by the various applied dc bias voltages.

Another argument against attributing t_d purely to transit time can be put forward by investigating the EL decay from a single-layer OLED after the voltage pulse is turned off (Fig. 7). The EL decay signal is nonexponential and can be described as the sum of two exponential decays. The first one with time constant $\tau_A \cong 0.3\,\mu$s is determined mainly by the RC time of the experimental setup (defined as 63% of the total value), whereas the second one with time constant $\tau_B \cong 10\,\mu$s clearly testifies to the existence of a delayed EL caused by the accumulation of charge carriers.

The presence of accumulated charges in the single-layer device is also manifested in the cell current at the end of the applied voltage pulse [Fig. 4(b)]. It takes more than 5 μs to discharge the device, compared to $\cong 1.5\,\mu$s required to reach the equilibrium current after the voltage pulse is turned on. So far we can only speculate where the charge-carrier accumulation takes place in the single-layer OLED. Possibly an interfacial layer is built up at the Mg:Ag cathode because of oxide formation, as previously reported for an ITO/poly(phenylphenylenevinylene) (PPPV)/Al device.[26] As our device fabrication was performed at pressures between 4×10^{-7} and 2×10^{-6} mbar rather than in ultrahigh vacuum (UHV), we cannot completely rule out that there are impurities in our OLEDs, e.g., oxygen, which can result in the buildup of such a thin interfacial layer between Alq_3 and Mg:Ag. Furthermore, it has been shown, both experimentally and theoretically, for different Alq_3–metal systems[56–58] that metals such as calcium, magnesium, and gold react with the Alq_3 to form an interfacial layer.

However, after the rectangular voltage pulse is turned off, the electrons have to pass through nearly the entire Alq_3 layer (100 nm) under a built-in potential of $\cong 1.2$ V to leave the device at the cathode. On their way back to the Mg:Ag electrode, the electrons may recombine radiatively with holes, which penetrated more deeply into the Alq_3 layer during the preceding voltage pulse on-phase, resulting in a delayed EL signal. Simulations by Ruhstaller[59] prove the existence of such a hole interpenetration inside the Alq_3 layer.

So far we have approached the goal of obtaining a value for the electron mobility in Alq_3 in an indirect way. Exact mobility determinations hence require TOF studies. Charge-carrier transport in amorphous organic solids has been extensively studied in the past two decades[48] because these materials have been widely used as photoreceptors in xerographic applications. Even the transport in Alq_3 has been investigated by TOF measurements.[55,60,61] However, only little information exists concerning TOF studies under operation conditions of OLEDs, i.e., in typically 100-nm-thick devices, and at electric fields $\geqslant 10^6$ V/cm. Moreover, it is illegitimate to conclude from the results obtained with thick (μm) to thin ($\cong$100 nm) devices because the morphology of thin and thick films can vary, and the transport in thin layers is expected to be dispersive because the carrier thermal equilibration time within the density of states (DOS) is longer than the transit time. A typical dispersive TOF signal obtained from an ITO/Alq_3 (150 nm)/rubrene (10 nm)/Mg:Ag device is shown in Fig. 8. A thin rubrene layer was used as CGL to ensure that a thin charge-carrier packet was generated and, because of the applied electric field, subsequently injected into the Alq_3 film. In the case of dispersive transport, t_{tr} is normally defined by the intersection of asymptotes to the plateau and trailing edge of the measured current transient in a double logarithmic representation as shown in Fig. 8(b). This analysis differs from those used in most theories of charge transport in amorphous organic semiconductors.[48] In these theories the transit time is defined as the average arrival time ($t_{1/2}$), which is the time required for the current to decrease to one-half of its value at the transit time [see also Fig. 8(b)]. Transit times calculated in this manner are typically two to three times those determined by the intersection of the asymptotes. However, in our case of dispersive TOF transients the mobility determination via $t_{1/2}$ is the more appropriate method because $t_{1/2}$ is not characterized by the fastest charge carriers as t_{tr} is, and therefore we end up with more realistic (averaged) values for μ_e. The field dependence of μ_e calculated via $t_{1/2}$ is weak, and the absolute mobility values are comparable within a factor of 2 to those obtained via transient EL measurements. Figure 9 presents this comparison of TOF and transient EL data. A more precise look at the TOF results indicates that the field dependence of μ_e is similar to that of the multilayer OLED (transient EL studies, assuming a homogeneous electrical field within the entire device structure), whereas the absolute μ_e values are lower. In the μ_e calculations via t_d (transient EL data) one has to consider both the electric field and the ''Schubweg'' between cathode and recombination zone. The latter can be less than the Alq_3 layer thickness and therefore the resulting μ_e values are higher than those determined via TOF measurements. Furthermore, the absolute μ_e values (TOF data) are higher than those obtained from the single-layer structure (transient EL studies). These are further convincing arguments that charge-carrier accumulation has an influence on t_d in the single-layer OLED.

A comparison of our TOF data with literature results[55,60,61] is presented in Fig. 10. All published electron mobility values in Alq_3 obtained via TOF measurements show a pronounced electric-field dependence. In addition these mobilities vary over several orders of magnitude. None of these effects were observed in our studies. These discrepancies from our work and among the literature data themselves might be attributed to differences in the layer thickness of the films investigated, as pointed out earlier. To the best of our knowledge the TOF investigations presented in this work are the first which have been performed with only

150-nm-thick Alq_3 films, i.e., a film thickness commonly used in OLED devices. Note that the displayed literature data (Fig. 10) were calculated via t_{tr} and not via $t_{1/2}$. Furthermore, the deposition rate has a distinct influence on μ_e. It was recently found that the electron mobility in Alq_3 increases by about two orders of magnitude as the deposition rate decreases from 0.7 to 0.2 nm/s,[62] whereas we used a deposition rate of 0.1 nm/s.

V. CONCLUSIONS

We have presented transient EL measurements from ITO/CuPc (20 nm)/NPB (45 nm)/Alq_3 (50 nm)/Mg:Ag multilayer and ITO/Alq_3 (100 nm)/Mg:Ag single-layer OLEDs. In the multilayer device the EL onset is limited by accumulated charges (holes) at the internal organic–organic interface (NPB/Alq_3) for $F \leqslant 7.7\times10^5$ V/cm (case a) and $F \leqslant 1.8\times10^6$ V/cm (case b) and transport limited in the high-electric-field range [$F \geqslant 8.5\times10^5$ V/cm (case a) and $F \geqslant 2.0\times10^6$ V/cm (case b)]. For the single-layer system, experiments with various offset voltages and analysis of the EL decay behavior manifest that t_d is determined by the accumulation of charge carriers rather than by charge-carrier transport. Therefore the determination of μ_e in Alq_3 is possible only for various limiting cases and must be considered a rough approximation. More accurate μ_e values are obtained from TOF measurements, which were performed for the first time on only 150-nm-thick Alq_3 layers and electric fields of up to 1.3×10^6 V/cm. Furthermore, we proved that insertion of a thin CuPc buffer layer between ITO and NPB, the use of separate improved layers for electron and hole transport, and/or driving the devices with positive offset voltages yield a faster EL onset and rise, which are crucial parameters for the application of OLEDs in flat-panel displays.

ACKNOWLEDGMENTS

The authors are indebted to H. Schmidt for his assistance in realizing a computer-controlled experimental setup and M. Tschudy for his support with the device fabrication. We thank Dr. B. Ruhstaller for helpful discussions. This work has been supported by the Fonds der Chemischen Industrie.

[1] C. W. Tang and S. A. Van Slyke, Appl. Phys. Lett. **51**, 913 (1987).
[2] C. W. Tang, S. A. Van Slyke, and C. H. Chen, J. Appl. Phys. **65**, 3610 (1989).
[3] C. Adachi, T. Tsutsui, and S. Saito, Appl. Phys. Lett. **56**, 799 (1990).
[4] J. Kido, M. Kimura, and K. Nagai, Science **267**, 1322 (1995).
[5] T. Wakimoto, R. Murayama, K. Nagayama, Y. Okuda, H. Nakada, and T. Tohma, in Proceedings SID '96 International Symposium, Digest of Technical Papers, San Diego (1996), p. 849.
[6] H. Nakada and T. Tohma, in *Proceedings International Symposium on Inorganic and Organic Electroluminescence*, edited by R. H. Mauch and H.-E. Gumlich (Wissenschaft und Technik Verlag, Berlin, 1996), p. 385.
[7] H. Nakamura, C. Hosokawa, and T. Kusumoto, in *Proceedings International Symposium on Inorganic and Organic Electroluminescence*, edited by R. H. Mauch and H.-E. Gumlich (Wissenschaft und Technik Verlag, Berlin, 1996), p. 95.
[8] Y. Hamada, T. Sano, H. Fujii, Y. Nishio, H. Takahashi, and K. Skibata, Jpn. J. Appl. Phys., Part 1 **35**, 1339 (1996).
[9] For recent progress, see *Organic Electroluminescent Materials and Devices*, edited by S. Miyata and H. S. Nalwa (Gordon and Breach, Lausanne, 1997).
[10] W. Helfrich and W. G. Schneider, Phys. Rev. Lett. **14**, 229 (1965).
[11] D. F. Williams and M. Schadt, J. Chem. Phys. **53**, 3480 (1970).
[12] C. Hosokawa, H. Tokailin, H. Higashi, and T. Kusumoto, Appl. Phys. Lett. **60**, 1220 (1992).
[13] Y. Ohmori, C. Morishima, M. Uchida, and K. Yoshino, Jpn. J. Appl. Phys., Part 2 **31**, L568 (1992).
[14] C. Hosokawa, H. Tokailin, H. Higashi, and T. Kusumoto, Appl. Phys. Lett. **63**, 1322 (1993).
[15] P. Delannoy *et al.*, Synth. Met. **67**, 197 (1994).
[16] A. J. Pal, R. Österbacka, K.-M. Källman, and H. Stubb, Appl. Phys. Lett. **71**, 228 (1997).
[17] P. Ranke, I. Bleyl, J. Simmerer, D. Haarer, A. Bacher, and H. W. Schmidt, Appl. Phys. Lett. **71**, 1332 (1997).
[18] J. Kalinowski, N. Camaioni, P. Di Marco, V. Fattori, and A. Martelli, Appl. Phys. Lett. **72**, 513 (1998).
[19] G. Kranzelbinder, F. Meghdadi, S. Tasch, G. Leising, L. Fasoli, and M. Sampietro, Synth. Met. **102**, 1073 (1999).
[20] Y. Ohmori, N. Tada, Y. Kurosaka, and K. Yoshino, Synth. Met. **102**, 1099 (1999).
[21] A. Chowdhury and A. J. Pal, Synth. Met. **106**, 85 (1999).
[22] A. G. Mückl, S. Berleb, W. Brütting, and M. Schwoerer, Synth. Met. **111–112**, 91 (2000).
[23] K. Book, H. Bässler, V. R. Nikitenko, and A. Elschner, Synth. Met. **111–112**, 263 (2000).
[24] D. Braun, D. Moses, C. Zhang, and A. J. Heeger, Appl. Phys. Lett. **61**, 3092 (1992).
[25] D. Braun, D. Moses, C. Zhang, and A. J. Heeger, Synth. Met. **55–57**, 4145 (1993).
[26] H. Vestweber, J. Oberski, A. Greiner, W. Heitz, R. F. Mahrt, and H. Bässler, Adv. Mater. Opt. Electron. **2**, 197 (1993).
[27] H. Vestweber, R. Sander, A. Greiner, W. Heitz, R. F. Mahrt, and H. Bässler, Synth. Met. **64**, 141 (1994).
[28] S. Karg, V. Dyakonov, M. Meier, W. Rieß, and G. Paasch, Synth. Met. **67**, 165 (1994).
[29] S. Kirstein, G. Cohen, D. Davidov, U. Scherf, M. Klapper, K. Chmil, and K. Müllen, Synth. Met. **69**, 415 (1995).
[30] Y.-H. Tak, H. Vestweber, H. Bässler, A. Bleyer, R. Stockmann, and H.-H. Hörhold, Chem. Phys. **212**, 471 (1996).
[31] J. Pommerehne, H. Vestweber, Y.-H. Tak, and H. Bässler, Synth. Met. **76**, 67 (1996).
[32] D. R. Baigent, P. G. May, and R. H. Friend, Synth. Met. **76**, 149 (1996).
[33] Y.-H. Tak, J. Pommerehne, H. Vestweber, R. Sander, H. Bässler, and H.-H. Hörhold, Appl. Phys. Lett. **69**, 1291 (1996).
[34] H. Chayet, R. Pogreb, and D. Davidov, Phys. Rev. B **56**, R12702 (1997).
[35] T. Östergard, A. J. Pal, and H. Stubb, J. Appl. Phys. **83**, 2338 (1998).
[36] R. Österbacka, G. Juška, K. Arlauskas, A. J. Pal, K.-M. Källman, and H. Stubb, J. Appl. Phys. **84**, 3359 (1998).
[37] P. W. M. Blom and M. C. J. M. Vissenberg, Phys. Rev. Lett. **80**, 3819 (1998).
[38] A. J. Pal, T. Östergard, R. Österbacka, J. Puloheimo, and H. Stubb, IEEE J. Sel. Top. Quantum Electron. **4**, 137 (1998).
[39] N. Tessler, N. T. Harrison, D. S. Thomas, and R. H. Friend, Appl. Phys. Lett. **73**, 732 (1998).
[40] N. Tessler, N. T. Harrison, and R. H. Friend, Adv. Mater. **10**, 64 (1998).
[41] V. Savvateev, A. Yakimov, and D. Davidov, Adv. Mater. **11**, 519 (1999).
[42] M. C. J. M. Vissenberg and P. W. M. Blom, Synth. Met. **102**, 1053 (1999).
[43] D. J. Pinner, N. Tessler, and R. H. Friend, Synth. Met. **102**, 1108 (1999).
[44] D. J. Pinner, R. H. Friend, and N. Tessler, J. Appl. Phys. **86**, 5116 (1999).
[45] D. J. Pinner, R. H. Friend, and N. Tessler, Synth. Met. **111-112**, 257 (2000).
[46] V. R. Nikitenko, V. I. Arkhipov, Y.-H. Tak, J. Pommerehne, H. Bässler, and H.-H. Hörhold, J. Appl. Phys. **81**, 7514 (1997).
[47] V. R. Nikitenko, Y.-H. Tak, and H. Bässler, J. Appl. Phys. **84**, 2334 (1998).
[48] P. M. Borsenberger and D. S. Weiss, *Organic Photoreceptors for Imaging Systems* (Marcel Dekker, New York, 1992).
[49] C. Hosokawa, H. Higashi, H. Nakamura, and T. Kusumoto, Appl. Phys. Lett. **67**, 3853 (1995).
[50] S. A. VanSlyke, C. H. Chen, and C. W. Tang, Appl. Phys. Lett. **69**, 2160 (1996).
[51] H. Vestweber and W. Rieß, Synth. Met. **91**, 181 (1997).
[52] W. Brütting, H. Riel, T. Beierlein, and W. Rieß, J. Appl. Phys. (2000, submitted).

[53] H. Riel, W. Brütting, T. Beierlein, E. Haskal, P. Müller, and W. Rieß, Synth. Met. **111-112**, 303 (2000).
[54] C. W. Tang, private communication.
[55] R. G. Kepler, P. M. Beeson, S. J. Jacobs, R. A. Anderson, M. B. Sinclair, V. S. Valencia, and P. A. Cahill, Appl. Phys. Lett. **66**, 3618 (1995).
[56] S. T. Lee, X. Y. Hou, M. G. Mason, and C. W. Tang, Appl. Phys. Lett. **72**, 1593 (1998).
[57] V.-E. Choong, M. G. Mason, C. W. Tang, and Y. Gao, Appl. Phys. Lett. **72**, 2689 (1998).
[58] A. Curioni and W. Andreoni, Synth. Met. **111-112**, 299 (2000).
[59] B. Ruhstaller, S. A. Carter, S. Barth, H. Riel, W. Rieß, and J. C. Scott, J. Appl. Phys. (2000, submitted).
[60] B. Chen and S. Liu, Synth. Met. **91**, 169 (1997).
[61] T. Tsutsui, H. Tokuhisa, and M. Era, in *Polymer Photonic Devices*, edited by B. Kippelen and D. D. C. Bradley, Proc. SPIE, Vol. 3281 (SPIE, Bellingham, 1998), p. 230.
[62] B. J. Chen, W. Y. Lai, Z. Q. Gao, C. S. Lee, S. T. Lee, and W. A. Gambling, Appl. Phys. Lett. **75**, 4010 (1999).